CREATED USING THE RSC LaTeX PCCP ARTICLE TEMPLATE – SEE www.rsc.org/electronicfiles FOR DETAILS

Orientational dynamics of colloidal ribbons self-assembled from microscopic magnetic ellipsoids.†

Fernando Martinez-Pedrero,[*a,b] **Andrejs Cebers,**[c‡] **and Pietro Tierno**[a,b]

Received Xth XXXXXXXXXX 20XX, Accepted Xth XXXXXXXXX 20XX
First published on the web Xth XXXXXXXXXX 200X
DOI: 10.1039/b000000x

arXiv:1607.00256v1 [cond-mat.soft] 1 Jul 2016

We combine experiments and theory to investigate the orientational dynamics of dipolar ellipsoids, which self-assemble into elongated ribbon-like structures due to the presence in each particle of a permanent magnetic moment perpendicular to the long axis. Monodisperse hematite ellipsoids are synthesized via sol-gel technique, and arrange into ribbons in presence of static or time-dependent magnetic fields. We find that under an oscillating field, the ribbons reorient perpendicular to the field direction, in contrast with the behaviour observed under a static field. This observation is explained theoretically by treating a chain of interacting ellipsoids as a single particle with an orientational and demagnetizing field energy. The model allows describing the orientational behaviour of the chain and captures well its dynamics at different strengths of the actuating field. The understanding of the complex dynamics and assembly of anisotropic magnetic colloids is a necessary step towards controlling the structure formation which has direct applications in different fluid-based microscale technologies.

1 Introduction

Magnetic colloids are microscopic building blocks which can be assembled into extended structures due to their dipolar nature.[1] An applied field can be used to induce the particle assembly or to carefully control the spatial orientation of the collective system. The aggregation of these particles into extended or compact structures due to dipolar forces is a relatively fast process compared to conventional self-assembly strategies. This feature, combined with the anisotropic nature of dipolar interactions, make magnetic colloids rather appealing for fundamental studies related with self-organization,[2–8] propulsion[9–13] and dynamics[14–17] in a dissipative medium. On the application side, magnetic colloids find use in several contexts related with biomedicine,[18] microfluidics[19,20] and microrheology.[21,22] When the particle shape departs from the spherical one, the self-assembly behaviour of these particles under an external field is determined by the competition between magnetic interactions and geometrical constraints.[23,24] Examples of the complex and sometimes unexpected structures obtained with anisotropic magnetic colloids have been recently reported by various groups both in experiments[25–29] and numerical simulations.[30–37]

In this article we study the dynamics of overdamped ferromagnetic ellipsoids dispersed in water and subjected to static or oscillating magnetic fields. These anisotropic particles present a permanent magnetic moment perpendicular to their long axis, and they readily assemble into elongated structures due to dipolar forces. The long axis of these chains can be easily oriented via a static external field. However, when the applied field oscillates, the chains reorient perpendicular to the field direction. By neglecting the effect of chain flexibility and thermal fluctuations, we show that this behaviour can be explained using a general model formulated for describing the dynamics of an individual particle with a demagnetizing field energy. By using video microscopy and particle tracking routines, we measure the average orientation of the chain and use these experimental data to validate the theoretical predictions.

2 Experimental part

Hematite ellipsoids are prepared from condensed ferric hydroxide gel using the procedure developed by Sugimoto and coworkers.[38,39] In more detail, a sodium hydroxide solution (21.64 g of NaOH in 90 ml of high deionized water) is gradually added to an iron chloride hexahydrate solution (54.00 g $FeCl_3-6H_2O$ in 100 ml of high deionized water). During the mixing process, both solutions are vigorously stirred and the temperature increased till 75 °C. After $\sim$ 5min, a 10 ml aqueous solution containing 0.29 g of potassium sulfate (K_2SO_4) is added and the resulting dark brown mixture is stirred for another 5min. Finally, the mixture is hermeti-

† Electronic Supplementary Information (ESI) available: Two .MPEG4 videos showing the chain dynamics under an oscillating magnetic field. See DOI: 10.1039/b000000x/

[a] *Departament d'Estructura i Constituents de la Matèria, Universitat de Barcelona, 08028, Barcelona, Spain. E-mail: ptierno@ub.edu*
[b] *Institut de Nanociència i Nanotecnologia, Universitat de Barcelona, 08028, Barcelona, Spain.*
[c] *University of Latvia, Faculty of Physics and Mathematics, Zellu 23, LV-1002.*

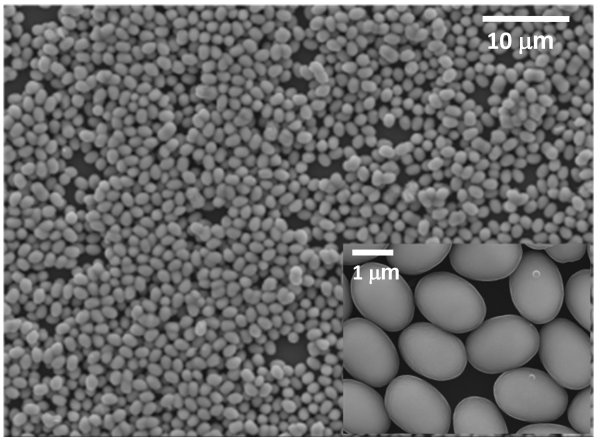

Fig. 1 Scanning electron microscopy image showing the monodisperse hematite ellipsoids. The inset displays a high magnification overview of the particles.

cally sealed and left unperturbed in an oven at 100 °C for 8 days. After this period, a dense aqueous suspension composed of monodisperse ellipsoids is obtained together with rod-like nanoparticles made of akaganeite, a precursor of the hematite. The ellipsoids are recovered by diluting the suspension with high deionized water, letting the particles sediment and removing the resulting yellowish-brown supernatant, a procedure that is repeated several times. After the synthesis, the hematite ellipsoids are functionalized with sodium dodecyl sulfate (SDS). This surfactant is grafted on the particle surface by dispersing the ellipsoids in an aqueous solution containing 0.12 g of SDS in 80 ml of high deionized water. Finally, the pH of the resulting solution is adjusted to $8.5-9.5$ by adding Tetramethylammonium Hydroxide (TMAH).

Particle size and shape were analyzed by scanning electron microscopy (SEM, Quanta 200 FEI, XTE 325/D8395). The ellipsoids dynamics were imaged with a CCD camera (Balser Scout scA640-74f, Basler) mounted on top of a light microscope (Eclipse Ni, Nikon) equipped with high magnification objectives. The applied magnetic field was provided by using two pairs of custom-made coils having a common axis located in the particle plane (x,y), and aligned along the x and y directions. A fifth coil was located under the sample cell to provide a perpendicular field along the z direction. AC fields were obtained by connecting the coils to a wave generator (TTi-TGA1244, TTi) feeding a power amplifier (IMG STA-800,stage line or BOP 10-20 M, KEPCO). The experiments were performed by confining a diluted water solution of the ellipsoids in a sealed rectangular capillary made of borosilicate glass (inner dimensions 0.10×2.00 mm, CMC Scientific).

3 Individual particle dynamics

As shown in the scanning electron microscopy (SEM) images of Fig.1, the synthetic approach described before allows to produce monodisperse prolate ellipsoids with a narrow size distribution, and characterized by a rather uniform shape. In particular, from the analysis of the SEM images we find that the particles present a major and minor axes of length $a = 1.80\mu m$ and $b = 1.33\mu m$, respectively. When dispersed in water, the ellipsoids sediment due to density mismatch, and float above the bottom glass plate showing a quasi two-dimensional confinement. Under no external field, we observe that these ellipsoids rapidly aggregate into chains due to the presence of a small permanent magnetic moment $\boldsymbol{m}$. However, in contrast to chains formed by paramagnetic ellipsoids,[26,40] the hematite particles arrange with their long axis perpendicular to the chaining direction, forming a ribbon-like structure, similar to those observed with magnetized Janus ellipsoids[28] or hematite peanut-shape particles.[41] The permanent moment perpendicular to the particle long axis (c-axis) can been explained by considering the magnetic structure of hematite, which crystallizes in the corundum structure.[42] In this arrangement, the iron cations are aligned antiferromagnetically along the c-axis, and above the Morin temperature, $T_M \sim 263$ K, the magnetic spins lay mostly in the basal plane, i.e. perpendicular to the c-axis.[41]

In order to measure the strength of the magnetic moment m, we apply a static field $\boldsymbol{H}$ and follow the reorientational motion of an ellipsoid, that was previously oriented in the perpendicular direction, Fig.2(a). The magnetic torque acting on the ellipsoid, $\boldsymbol{\tau}_m = \mu_w \boldsymbol{m}\times\boldsymbol{H}$ is balanced by the viscous torque arising from its rotation in the fluid, $\boldsymbol{\tau}_v = -\xi_r\dot{\boldsymbol{\theta}}$. Here μ_w denotes the magnetic susceptibility of water and ξ_r the rotational friction coefficient of the ellipsoid. By solving the torque balance equation written in the overdamped limit, $\boldsymbol{\tau}_m + \boldsymbol{\tau}_v = 0$, and taking into account that the angle between the permanent moment and the ellipsoid long axis is $\pi/2$, we arrive at

$$\theta(t) = 2\tan^{-1}\left[\tanh\left(\frac{t}{\tau_r}\right)\right], \qquad (1)$$

where $\tau_r = 2\xi_r/(\mu_w m H)$ is the relaxation time. The rotational friction coefficient for a prolate ellipsoid rotating around its short axis can be written as, $\xi_r = 8\pi\eta V_c f_r$,[43] where $\eta = 10^{-3}$Pa·s is the dynamic viscosity of the medium (water), $V_c = (4\pi ab^2)/3$ is the volume of the ellipsoid, and f_r is a geometrical factor which depends on the ellipsoid long and short axis.[40] Assuming $\mu_w \sim \mu_0 = 4\pi 10^{-7}$H m^{-1}, and an applied field value $H = 1100$A m^{-1} we obtain from the experimental data a relaxation time $\tau_r = 0.035$s, which corresponds to a particle magnetic moment $m = 2.2\cdot 10^{-16}$A m^2. This permanent moment corresponds to a spontaneous magnetization of the ellipsoid $M = 138$A m^{-1}, which is actually one order

This journal is © The Royal Society of Chemistry [year]

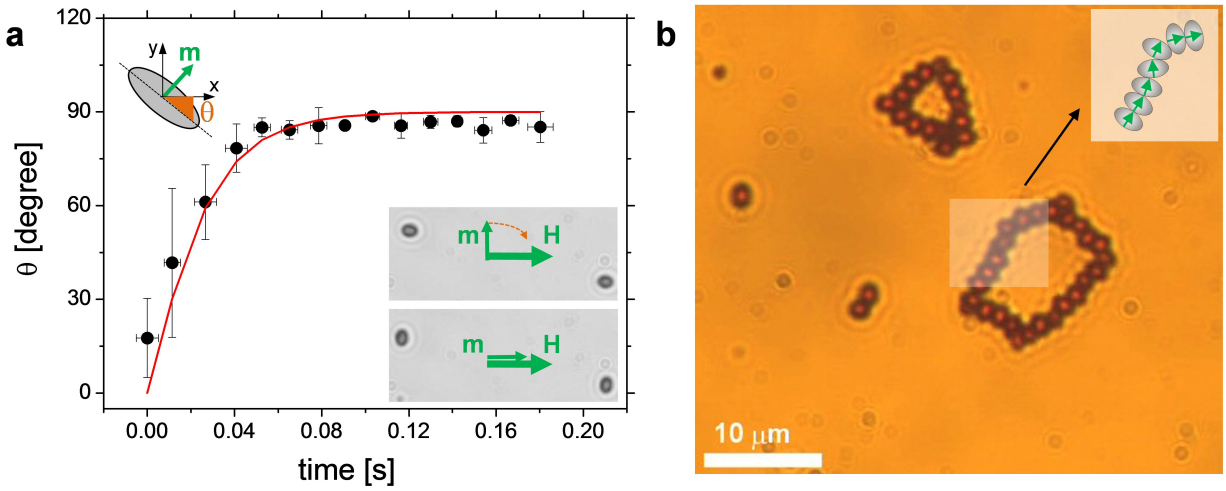

Fig. 2 (a) Angle θ between the ellipsoid long axis and the x axis versus time for an applied field of amplitude $H = 1100\,\mathrm{A\,m^{-1}}$. The continuous red line is a fit of Eq.1 in the main text. As shown in the inset, under the constant field $\boldsymbol{H}$ applied along the x direction, the ellipsoids reorient with their magnetic moments along the field. (b) Optical microscope image showing two rings of dipolar ellipsoids spontaneously assembled after compensating the earth magnetic field. The small schematic on the top-right corner shows a section of one ring composed by ellipsoids having permanent moments perpendicular to their long axis.

of magnitude lower than the maximum spontaneous magnetization value for hematite in the bulk,[44] $M_s = 2\mathrm{kA\,m^{-1}}$. This discrepancy can be attributed to several factors arising during the synthesis process. It should be noted that our ellipsoids are not coated with a silica layer which prevents oxidation of the outer surface. A discrepancy with the bulk magnetization of hematite was found in other works,[45,46] where smaller hematite particles were studied.

4 Rings and ribbons

The permanent moments within the ferromagnetic ellipsoids are able to induce chaining due to dipolar interactions between the particles. In absence of any applied field, these chains already have the tendency to orient along the direction determined by the weak earth magnetic field ($\sim 50\mu T$). In order to eliminate the influence of this field, we apply a small static field in the opposite direction. When matching the amplitude of the earth field, the ellipsoids form chains pointing along random directions, or close into rings, as those shown in Fig.2(b). The formation of rings from interacting dipolar particles has been observed with Janus ellipsoids[28], and was previously predicted as a low energy state of different magnetized particles.[47–50] Given the small size of our ellipsoids, the shape of the rings continuously fluctuates due to thermal motion of the individual units, and the rings can easily break or reform with time. However, we find that the application of an oscillating field along the z direction is able to keep the ring stable over time.

We next study the orientation and dynamics of the former structures under an applied field in the (x,y) plane. For a static field, single ellipsoids and ribbons orient as expected, i.e. parallel to the field direction. In contrast, an oscillating field of amplitude H and angular frequency ω, $\boldsymbol{H} = H\cos(\omega t)\boldsymbol{e}_y$, produces exactly the opposite scenario, i.e. the ribbons orient in the perpendicular direction, as shown in Fig.3(a). We compare this response with the behaviour of commercial paramagnetic colloids having diameter $1\mu m$ (Dynabeads Myone, Dynal), which are isotropic particles that have an induced moment rather than a permanent one. In the latter case we find that the particles form chains along the field direction as expected, for both static and oscillating fields. In a mixture of paramagnetic spherical particles and ferromagnetic ellipsoids, Fig.3(b), we find that the AC field induces formation of chains composed by paramagnetic particles, which orient parallel to the applied field, and chains composed by the ferromagnetic ellipsoids which orient in the perpendicular direction. The system thus assembles into a square-like network,that resembles to those formedby orthogonal dipoles[29]. When the field is switched off, the chains of paramagnetic colloids disintegrate because of thermal forces. In contrast, the chains of ellipsoids remain since they are kept together by strong dipolar forces. However, their mean orientations fluctuate due to thermal forces.
In order to explore the reorientational dynamics of the ribbons, we start by analyzing the fraction of particles ϕ having an average orientation θ, considering only elementary units such as single ellipsoids, dimers and trimers, Fig.3(c). In absence of field (deshed lines) monomers, dimers or trimers dis-

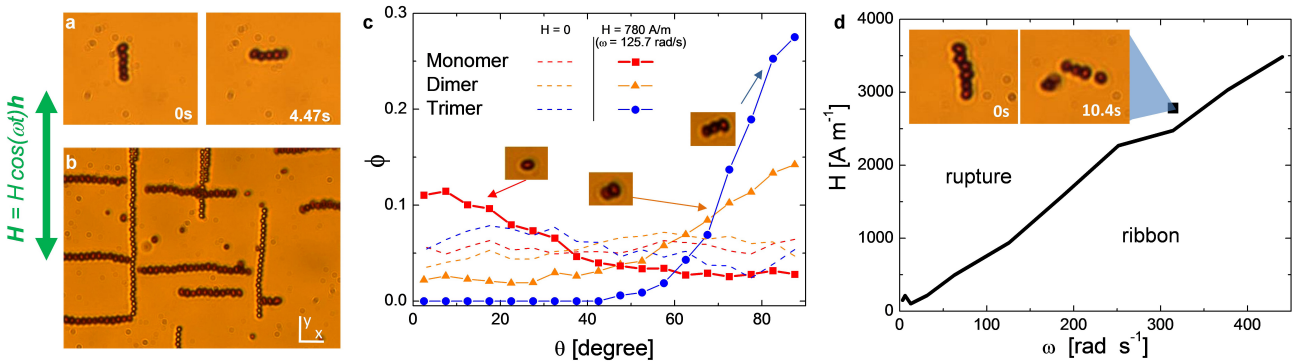

Fig. 3 (a) Two images showing a ribbon of hematite ellipsoids reorienting perpendicular to the direction of an oscillating field direction. The applied field has amplitude $H_0 = 1600\,\mathrm{A\,m^{-1}}$ and angular frequency $\omega = 314.1\,\mathrm{rad\,s^{-1}}$. The corresponding video (see MovieS1) can be found in the Supporting Information (SI). (b) Microscope image showing the orientation of ribbons (darker particles) and chains of paramagnetic colloids (lighter particles) subjected to an oscillating field oriented along the y direction. (c) Fraction ϕ of particles with a given orientation θ in absence of field (dashed lines) and in presence of an oscillating field with amplitude $H_0 = 780\,\mathrm{A\,m^{-1}}$ and angular frequency $\omega = 125.7\,\mathrm{rad\,s^{-1}}$ (filled points). (d) Dynamic state diagram in the (ω, H) plane. The video corresponding to the inset (MovieS2) can be found in the SI.

play the same average behaviour, with no preferred orientation. The filled points in Fig.3(c) indicate the behaviour of the various species under an applied field oscillating with angular frequency $\omega = 314.1\,\mathrm{rad\,s^{-1}}$ and amplitude $H = 1600\,\mathrm{A\,m^{-1}}$. Once the AC field is applied along the y direction, the monomers are able to follow the field synchronously and oscillate periodically around their long axis. The driving mechanism for this behaviour is the torque exerted on the ellipsoids by the oscillatory field. Consequently, a high fraction of ellipsoids orients at small θ. As the length of the ribbon increases, the composite structures show a larger tendency to orient with the chain axis perpendicular to the field, where θ becomes larger. Larger agregates like trimers require a higher torque to stand up above the plane in order to follow the field modulations because of the increase in the rotational friction coefficient. Thus at parity of applied field, the more elongated structures show the opposite behaviour, and reorient in the horizontal (x,y) plane, MovieS1 in the Supporting Information (SI). Fig.3(d) shows the dynamic state diagram, separating the region in the (ω, H) plane where long ribbons orients perpendicular to the field ("ribbon" region), from the region where the ribbons break into pieces. The latter behaviour arises since at high field strengths the magnetic torque exerted by the field is able to induce the rotation of monomers and dimers within the ribbons. A video illustrating this process (MoviS2) can be found in the Supporting Information. At very low angular frequencies, $\omega < 12.5\,\mathrm{rads^{-1}}$, the ribbon are able to follow synchronously the applied field, and perform oscillations which avoid the perpendicular orientation.

5 Theoretical model

The dipolar energy of a chain made of homogeneously magnetized ellipsoids with magnetization M can be modelled as an effective demagnetizing field energy, in the approximation that all magnetic moments of particles are equal. The energy per volume can be written as:

$$\frac{E}{V} = -M(\boldsymbol{e}\cdot\boldsymbol{H}) - \frac{\Delta N}{2}M^2(\boldsymbol{e}\cdot\boldsymbol{n})^2\,, \qquad (2)$$

$\boldsymbol{e}$ and $\boldsymbol{n}$ being the unit vectors aligned along the permanent moment and the chain axis directions, respectively. Eq. 2 was originally formulated by Stoner and Wohlfarth[51] to describe the equilibrium direction of a uniformly magnetized ellipsoid subjected to an external field. The first term represents the energy associated with the applied field, being $\boldsymbol{e}\cdot\boldsymbol{H}$ proportional to the cosine of the angle between the permanent moment of the ellipsoid and the external field. The second term in Eq. 2 describes the energy per volume associated with the demagnetizing field, being $\boldsymbol{e}\cdot\boldsymbol{n}$ the cosine of the angle between the permanent moment of the ellipsoid and the previously referred chain longest axis. The demagnetized factor $\Delta N = N_\perp - N_\parallel$ of a chain of n particles is given by (see Appendix A):

$$\Delta N = \pi\left(\zeta(3) + \frac{1}{2}\psi^{(2)}(n) - \frac{1}{n}\left(\frac{\pi^2}{6} - \psi^{(1)}(n)\right)\right) \qquad (3)$$

where subscripts $\parallel$, $\perp$ denote the parallel and perpendicular components to the symmetry axis of the ellipsoid, respectively. In Eq. 3 ζ is the zeta function, ψ the digamma function and $\psi^{(i)}$ its derivative of order i. Eq. 2 has been used in the past to study the optical anisotropy of magnetic colloids in AC

This journal is © The Royal Society of Chemistry [year]

fields.[52,53] The governing equations for the particle are:

$$\boldsymbol{K_e} E = 0 \tag{4}$$

$$-\xi \boldsymbol{n} \times \dot{\boldsymbol{n}} - \boldsymbol{K_n} E = 0 \tag{5}$$

where ξ is the rotational friction coefficient of the ribbon, and $\boldsymbol{K_a} = \boldsymbol{a} \times \frac{\partial}{\partial \boldsymbol{a}}$. We assume that, at relatively high frequency, the magnetic equilibrium is established much faster as compared to the evolution of the particle orientation given by the director $\boldsymbol{n}$. We next assume that the external field oscillates as $\boldsymbol{H} = H\cos(\omega t)\boldsymbol{h}$, with $\boldsymbol{h} = (1,0)$. In this case the characteristic time of particle orientation $\tau_r = \xi_r \Delta N / H^2 V >> 1/\omega$ is much greater than the period of the AC field, and Eq. 5 can be solved by separating slow and fast time scales. By taking the time average with respect to the fast oscillation of the AC field we obtain (Appendix B):

$$-\xi \boldsymbol{n} \times \dot{\boldsymbol{n}} = \frac{1}{2} \frac{H^2 V}{\Delta N} \boldsymbol{n} \cdot \boldsymbol{h} [\boldsymbol{n} \times \boldsymbol{h}]. \tag{6}$$

Introducing the direction angle ϑ as, $\boldsymbol{n} = (\cos(\vartheta), \sin(\vartheta))$; $\dot{\boldsymbol{n}} = (-\sin(\vartheta), \cos(\vartheta))\dot{\vartheta}$, Eq. 6 can be written as:

$$\dot{\vartheta} = \frac{\omega_c}{2\omega h_a^2} \cos(\vartheta)\sin(\vartheta), \tag{7}$$

where $h_a = \Delta N M / H$ describes the ratio of the effective demagnetizing field strength and the applied field strength and $\omega_c = \Delta N M^2 V / \xi$ is the critical frequency of the particle motion. The time is rescaled according to $\tilde{t} = \omega t$. Eq. 7 has two stationary points at $\vartheta = 0$ and $\vartheta = \pi/2$. It is easy to see that the first is unstable, while the last is stable. Thus, for small AC fields the particle orients in the direction perpendicular to the field, and the solution of Eq. 7 reads as

$$\tan(\vartheta(\tilde{t})) = \tan(\vartheta(0)) \exp(\omega_c \tilde{t} / (2\omega h_a^2)), \tag{8}$$

and the (x,y) components of the director $\boldsymbol{n}$ are:

$$n_x(\tilde{t}) = \frac{1}{\sqrt{1 + \tan^2(\vartheta(0)) \exp(\omega_c \tilde{t} / (\omega h_a^2))}} \tag{9}$$

$$n_y(\tilde{t}) = \frac{\tan(\vartheta(0)) \exp(\omega_c \tilde{t} / (2\omega h_a^2))}{\sqrt{1 + \tan^2(\vartheta(0)) \exp(\omega_c \tilde{t} / (\omega h_a^2))}} \tag{10}$$

We point out that Eq. 2 contains the effect of the dipolar interaction between the particles, since as shown in Appendix A, the demagnetizing field energy can be derived from the dipolar energy. The general case considering large field amplitude is more complex and out of the scope of this article, it will be treated in a separate work.

6 Discussion and conclusions

The model introduced in the previous section allows explaining the ribbon orientation perpendicular to the applied field. With no applied field, the magnetic energy of a chain of dipoles is minimal when these dipoles are oriented along the chain axis in the head to tail configuration. A coherent deviation of the magnetic moments of the particles from the direction of chain axis will increase the dipolar energy. As shown in Appendix A, this situation is similar to the increase of the demagnetizing energy of an homogeneously magnetized ellipsoid when the magnetization direction deviates from the direction of its long axis. Under an external field, the direction of the dipoles in the chain is determined by the interaction with the field and by the effective anisotropy field along the chain axis, Eq. 2 of the model.

If the applied field oscillates, the chain will try to reorient along the field direction. However when the period of the applied field is small compared with the characteristic reorientation time of the chain, the chain will not follow the field. In this situation, during a semi-period the applied field will point in the opposite direction with respect to the dipole moments in the chain, and this will raise the magnetic energy of chain. In order to reduce this energetic contribution, the chain will tend to orient perpendicular to the applied field.

In Fig.4 we show the results from an average over more than 15 experiments where we measure the evolution of the n_y component for a ribbon composed by 4 ellipsoids. The latter are subjected to an external oscillating field oriented along the x axis and at different amplitudes of the applied field (angular frequency $\omega = 314.1 \mathrm{rad\,s^{-1}}$). In all the experiments the earth magnetic field was compensated and the ribbons were initially oriented along the x direction. In agreement with the behaviour predicted by Eq. 10, as time proceeds the chains align perpendicular to the direction of the applied field, and the process speeds up by increasing the field amplitude. The compact ribbons behave as rods composed by four stacked ellipsoids, thus having a total length $L = 4b$, a diameter a and a corresponding rotational friction coefficient $\xi = \frac{\pi \eta L^3}{3 \log[L/a]}$. We fit the experimental data with Eq. 10, using the initial chain orientation, $\tan(\vartheta(0))$, and the ratio $\beta \equiv \omega_c / h_a^2$ as adjustable parameters. In particular we use a multiple fit taking $\tan(\vartheta(0))$ as a common parameter and extracting the dependence $\beta = \beta(H)$, which is showed in the inset of Fig.5. We use these results to estimate the demagnetization factor, which in International System units is $\Delta N = \frac{\mu_w V_c}{4\pi \xi \beta} = 3.2$. Eq. 3 gives a similar value of $\Delta N \cong 2.6$. It should be noted that ΔN is calculated using the approximation of a chain of spherical particles and assuming that the field generated by each particle is equal to the field generated by a dipole located at the particle center. Considering ellipsoids rather than spherical particles would only introduce a small correction to the demagnetization factor since the ratio between the long and the short axis $a/b = 0.7$ is close to one. We also note that longer chains composed by a higher number of ellipsoids behave qualitatively in

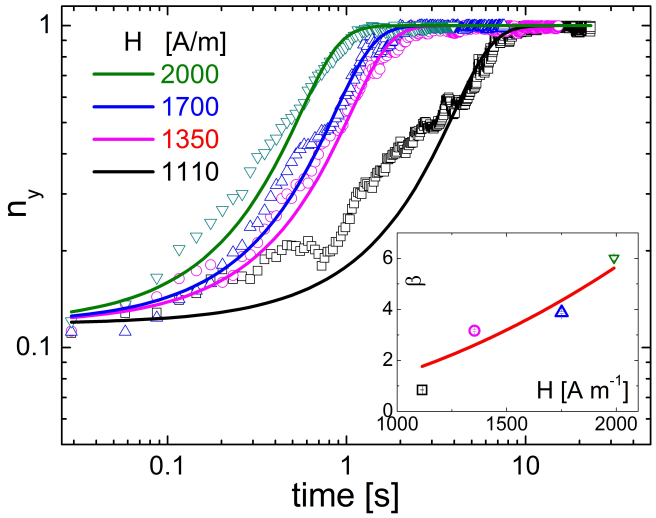

Fig. 4 Log-Log plot of the n_y component for a ribbon subjected to a magnetic field oscillating along the x direction with angular frequency $\omega = 314.1\text{rad}\,\text{s}^{-1}$ and different amplitudes. Continuous lines are fit following Eq. 10 in the text. Inset: variation of the parameter $\beta \equiv \omega_c/h_a^2$ obtained from the fits in the main panel versus field strength H. The continuous red line is $\beta \sim H^2$.

the same way, although the corresponding increase in the rotational friction coefficient favours bending and later rupture of the chain.

In conclusion, we studied experimentally and theoretically the orientational dynamics of interacting ferromagnetic ellipsoids subjected to static and time dependent magnetic fields. The presented model explains the observed behavior where chains of dipolar particles orient perpendicular to the direction of the oscillating field. A similar feature will occur for spherical ferromagnetic particles when the flexibility of the magnetic filament favours its orientation perpendicularly to the AC field.[54,55] It has also been reported in other soft matter systems which use ferromagnetic particles,[56] thus our findings can be useful for different systems. On the application side, ferromagnetic particles subjected to AC field are often encountered in magnetorheological and ferrofluid systems. For example, heating can be induced in ferromagnetic materials by exposing them to high frequency magnetic fields. This technique known as "magnetic hyperthermia" is used to destroy dangerous cells infecting tissues in living systems.[57] Moreover, the possibility to remotely control microscopic chains and their assembly/disassembly under an external field can be useful for microfluidics systems. In this context, optically trapped chains of colloidal silica particles have been used to displace fluids into customized microscopic channels.[58] More work in these directions have been done with magnetic colloids,[59–62] since low frequency magnetic fields can actuate over particles without unwanted heating effect such as those caused by adsorption of focalized laser light. Examples of mechanical stirrers composed by chains of paramagnetic colloids have been developed by several groups.[63–67] Our approach could provide further functionality to these systems, since the orientation of the chains can be controlled via the use of both static or time dependent magnetic fields. Finally, the ability to align anisotropic structures perpendicular to the external field gives new possibilities for microrheological measurements.[68]

Appendix

A Derivation of the demagnetization energy from dipolar interactions

In the continuum approximation the magnetic field created by a given magnetization distribution $\boldsymbol{M}(\boldsymbol{r})$ is:

$$\boldsymbol{H}(\boldsymbol{r}) = -\nabla_{\boldsymbol{r}} \int\int \frac{\boldsymbol{M}(\boldsymbol{r}')\cdot(\boldsymbol{r}-\boldsymbol{r}')}{|\boldsymbol{r}-\boldsymbol{r}'|^3} d\boldsymbol{r}' \,. \tag{11}$$

The corresponding dipolar energy reads as:

$$E_d = -\frac{1}{2}\int \boldsymbol{M}(\boldsymbol{r})\boldsymbol{H}(\boldsymbol{r}) d\boldsymbol{r} \,. \tag{12}$$

Taking into account that:

$$\frac{\boldsymbol{r}-\boldsymbol{r}'}{|\boldsymbol{r}-\boldsymbol{r}'|^3} = \nabla_{\boldsymbol{r}'}\frac{1}{|\boldsymbol{r}-\boldsymbol{r}'|} \,.$$

Eq. 11 can be expressed as:

$$\boldsymbol{H}(\boldsymbol{r}) = \nabla_{\boldsymbol{r}}\Big(-\int \frac{M_n(\boldsymbol{r}')}{|\boldsymbol{r}-\boldsymbol{r}'|} dS' + \int \frac{div(\boldsymbol{M}(\boldsymbol{r}'))}{|\boldsymbol{r}-\boldsymbol{r}'|} d\boldsymbol{r}'\Big) \,, \tag{13}$$

where M_n is the surface magnetization. For an ellipsoid with uniform magnetization ($div(\boldsymbol{M}) = 0$) and the first term gives the homogeneous field in the particle body, that can be expressed in terms of the demagnetizing field coefficients. For an ellipsoid of revolution of volume V, $H_{\parallel} = -N_{\parallel}M_{\parallel}$ and $H_{\perp} = -N_{\perp}M_{\perp}$, where subscripts $\parallel,\perp$ denote the components parallel and perpendicular to the symmetry axis of ellipsoid, respectively. As a result the dipolar interaction energy reads as:

$$E_d = \frac{V}{2}(N_{\parallel}M_{\parallel}^2 + N_{\perp}M_{\perp}^2) \,. \tag{14}$$

In the case of a chain of N dipoles, the dipolar energy (Eq.12) can be expressed as follows:

$$E_d = -\frac{1}{2}\sum_{j\neq i} \boldsymbol{m}_i \boldsymbol{H}_{ij} \tag{15}$$

where,

$$\boldsymbol{H}_{ij} = -\frac{\boldsymbol{m}_j}{|\boldsymbol{r}_{ij}|^3} + \frac{3\boldsymbol{r}_{ij}(\boldsymbol{m}_j\cdot\boldsymbol{r}_{ij})}{|\boldsymbol{r}_{ij}|^5} \tag{16}$$

This journal is © The Royal Society of Chemistry [year]

$\boldsymbol{m}_i$ is the magnetic moment of particle i, and $\boldsymbol{r}_{ij}$ is the radius vector between the particles i and j. If all the magnetic moments in the chain are equal, we can write:

$$E_d = \sum_{i=1}^{N-1} \sum_{j=i+1}^{N} \Big(\frac{\boldsymbol{m}^2}{|\boldsymbol{r}_{ij}|^3} - \frac{3(\boldsymbol{m}\cdot\boldsymbol{n})^2}{|\boldsymbol{r}_{ij}|^3} \Big). \quad (17)$$

For an ensemble of spherical particles having diameter d, the dipolar interaction energy reads as:

$$E_d = -3m^2(\boldsymbol{e}\cdot\boldsymbol{n})^2 \sum_{i=1}^{N-1} \sum_{j=i+1}^{N} \frac{1}{r_{ij}^3} = -3m^2(\boldsymbol{e}\cdot\boldsymbol{n})^2 \frac{1}{d^3} \sum_{l=1}^{N-1} \frac{N-l}{l^3}$$

where $\boldsymbol{n}$ denotes the unit vector along the axis of the chain and $\boldsymbol{e}$ is the unit vector along the magnetic moments of the particles. Since the total volume of the chain is $V = \pi N d^3/6$ we obtain:

$$E_d = -\frac{\pi}{2} M^2 V \frac{(\boldsymbol{e}\cdot\boldsymbol{n})^2}{N} \sum_{l=1}^{N-1} \frac{N-l}{l^3} \quad (18)$$

The sum can be expressed through digamma and zeta functions as:

$$\frac{1}{N} \sum_{l=1}^{N-1} \frac{N-l}{l^3} = \zeta(3) + \frac{1}{2}\psi^{(2)}(N) - \frac{1}{N}\Big(\frac{\pi^2}{6} - \psi^{(1)}(N)\Big) \quad (19)$$

where $\psi^{(i)}(x)$ is the i order derivative of the digamma function $\psi(x)$. Finally we obtain Eq.3 of the main text.

B Derivation of Equation 6 in the text

By considering a small amplitude of the field $\boldsymbol{H}$, one can find a solution of Eq. 4 using the power series: $\boldsymbol{e} = \boldsymbol{e}_0 + \boldsymbol{e}_1 + \boldsymbol{e}_2$. The zero order solution is $\boldsymbol{e}_0 = \boldsymbol{n}$ and the condition $\boldsymbol{e}^2 = 1$ gives $\boldsymbol{e}_0 \cdot \boldsymbol{e}_1 = 0$, and $\boldsymbol{e}_0 \cdot \boldsymbol{e}_2 = -\boldsymbol{e}_1^2/2$. Up to the second order term $\boldsymbol{e}\cdot\boldsymbol{n} = 1 + \boldsymbol{e}_2\cdot\boldsymbol{n}$ and Eq. 4 reads as:

$$-MH\cos(\omega t)\boldsymbol{e}\times\boldsymbol{h} - \Delta N M^2 \boldsymbol{e}\cdot\boldsymbol{n}[\boldsymbol{e}\times\boldsymbol{n}] = 0.$$

This expression in the first order gives:

$$-MH\cos(\omega t)\boldsymbol{e}_0\times\boldsymbol{h} - \Delta N M^2[\boldsymbol{e}_1\times\boldsymbol{n}] = 0, \quad (20)$$

and up to the second order,

$$-MH\cos(\omega t)\boldsymbol{e}_1\times\boldsymbol{h} - \Delta N M^2[\boldsymbol{e}_2\times\boldsymbol{n}] = 0.$$

Eq. 20 can be rewritten as:

$$\boldsymbol{e}_1 = -\frac{MH\cos(\omega t)[\boldsymbol{n}\times[\boldsymbol{n}\times\boldsymbol{h}]]}{\Delta N M^2}, \quad (21)$$

and Eq. 4 in the main text as:

$$-\xi\boldsymbol{n}\times\dot{\boldsymbol{n}} = -\Delta N M^2 V \boldsymbol{e}\cdot\boldsymbol{n}[\boldsymbol{n}\times\boldsymbol{e}]. \quad (22)$$

By considering terms up to the second order,

$$-\xi\boldsymbol{n}\times\dot{\boldsymbol{n}} = -\Delta N M^2 V[\boldsymbol{n}\times\boldsymbol{e}_1 + \boldsymbol{n}\times\boldsymbol{e}_2]. \quad (23)$$

As a result, Eq. 23 reduces to:

$$-\xi\boldsymbol{n}\times\dot{\boldsymbol{n}} = -\Delta N M^2 V \boldsymbol{n}\cdot\boldsymbol{e}_1 - MH\cos(\omega t)V[\boldsymbol{e}_1\times\boldsymbol{h}] \quad (24)$$

Finally, using Eq. 21 we have:

$$\xi\boldsymbol{n}\times\dot{\boldsymbol{n}} = \Delta N M^2 V\Big\{\boldsymbol{n}\cdot\boldsymbol{e}_1 - \Big(\frac{H\cos(\omega t)}{\Delta N M}\Big)^2[[\boldsymbol{n}\times[\boldsymbol{n}\times\boldsymbol{h}]]\times\boldsymbol{h}]\Big\}$$

In the slow time scale of the particle motion this equation reduces to Eq.6 in the main text by taking the average with respect to one period of the AC field.

C Acknowledgements

F. M.P. and P. T. acknowledge support from the European Research Council Project No. 335040. A. C. acknowledge support from National Research Programme No. 2014.10-4/VPP-3/21. P. T. acknowledges support from the "Ramon y Cajal" Program No. RYC-2011-07605, from Mineco (Grant No. FIS2013-41144-P), and AGAUR (Grant No. 2014SGR878).

References

1 *Ferrohydrodynamics*, ed. R. E. Rosensweig, Dover, New York, 1997.
2 T. Tlusty and S. A. Safran, *Science*, 2000, **290**, 1328.
3 N. Osterman, I. Poberaj, J. Dobnikar, D. Frenkel, P. Ziherl and D. Babic, *Phys. Rev. Lett.*, 2009, **103**, 228301.
4 S. K. Smoukov, S. Gangwal, M. Marquez and O. D. Velev, *Soft Matter*, 2009, **5**, 1285.
5 R. M. Erb, H. S. Son, B. Samanta, V. M. Rotello and B. B. Yellen, *Nature*, 2009, **457**, 999.
6 A. Snezhko and I. S. Aranson, *Nat. Materials*, 2011, **10**, 698.
7 J. Yan, M. Bloom, S. C. Bae, E. Luijten and S. Granick, *Nature*, 2012, **491**, 578.
8 J. Yan, S. C. Bae and S. Granick, *Soft Matter*, 2015, **11**, 147.
9 R. Dreyfus, J. Baudry, M. L. Roper, M. Fermigier, H. A. Stone and J. Bibette, *Nature*, 2005, **437**, 862.
10 A. Cebers, *Magnetohydrodynamics*, 2005, **41**, 63.
11 H. Morimoto, T. Ukai, Y. Nagaoka, N. Grobert and T. Maekawa, *Phys. Rev. E*, 2008, **78**, 021403.
12 P. Tierno, R. Golestanian, I. Pagonabarraga and F. Sagués, *Phys. Rev. Lett.*, 2008, **101**, 218304.
13 N. Casic, N. Quintero, R. A. Nodarse, F. G. Mertens, L. Jibuti, W. Zimmermann and T. M. Fischer, *Phys. Rev. Lett.*, 2013, **110**, 168302.
14 P. Tierno, R. Muruganathan and T. M. Fischer, *Phys. Rev. Lett.*, 2007, **98**, 028301.
15 J. Jordanovic, S. Jäger and S. H. L. Klapp, *Phys. Rev. Lett.*, 2011, **106**, 038301.
16 J. Dobnikar, A. Snezhko and A. Yethiraj, *Soft Matter*, 2013, **9**, 3693.
17 J. E. Martin and A. Snezhko, *Rep. Prog. Phys.*, 2013, **76**, 126601.
18 *Scientific and Clinical Applications of Magnetic Carriers*, ed. U. Häfeli, W. Schütt, J. Teller and M. Zborowski, Plenum Press, New York, 1997.
19 M. A. M. Gijs, F. Lacharme and U. Lehmann, *Chem. Rev.*, 2010, **110**, 016001.

20 F. Martinez-Pedrero and P. Tierno, *Phys. Rev. Applied*, 2015, **3**, 051003.
21 C. Goubault, P. Jop, M. Fermigier, J. Baudry, E. Bertrand and J. Bibette, *Phys. Rev. Lett.*, 2003, **91**, 260802.
22 P. Dhar, Y. Cao, T. M. Fischer and J. A. Zasadzinski, *Phys. Rev. Lett.*, 2010, **104**, 016001.
23 D. Zerrouki, J. Baudry, D. Pine, P. Chaikin and J. Bibette, *Nature*, 2008, **455**, 380.
24 P. Tierno, *Phys. Chem. Chem. Phys.*, 2014, **16**, 23515.
25 A. K. F. Dyab, M. Ozmen, M. Ersoz and V. N. Paunov, *J. Mater. Chem.*, 2009, **19**, 3475.
26 O. Guell, F. Sagues and P. Tierno, *Adv. Mater.*, 2011, **23**, 3674.
27 S. Sacanna, L. Rossi and D. J. Pine, *J. Am. Chem. Soc.*, 2012, **134**, 6112.
28 J. Yan, K. Chaudhary, S. C. Bae, J. A. Lewis and S. Granick, *Nat. Commun.*, 2013, **4**, 1516.
29 B. Bharti and O. D. Velev, *Langmuir*, 2015, **31**, 7897.
30 S. C. McGrother, A. Gil-Villegas and G. Jackson, *Mol. Phys.*, 1998, **95**, 657.
31 S. Kantorovich, R. Weeber, J. J. Cerda and C. Holm, *Soft Matter*, 2011, **7**, 5217.
32 C. E. Alvarez and S. H. L. Klapp, *Soft Matter*, 2012, **8**, 3480.
33 C. E. Alvarez and S. H. L. Klapp, *Soft Matter*, 2013, **9**, 8761.
34 A. I. Abrikosov, S. Sacanna, A. P. Philipse and P. Linse, *Soft Matter*, 2013, **9**, 8904.
35 J. G. Donaldson, E. S. Pyanzina, E. V. Novak and S. S. Kantorovich, *J. Magn. Magn. Mat.*, 2015, **383**, 267.
36 F. Kogler, O. D. Velev, C. K. Hall and S. H. L. Klapp, *Soft Matter*, 2015, **11**, 7356.
37 J. M. Dempster, R. Zhang and M. O. de la Cruz, *Phys. Rev. E*, 2015, **92**, 042305.
38 T. Sugimoto, M. M. Khan and M. Muramatsu, *Colloids Surf. A*, 1993, **70**, 167.
39 L. Rossi (2012). Colloidal Superballs (doctoral thesis). Utrecht University, Utrecht, Holland.
40 P. Tierno, J. Claret, F. Sagués and A. Cebers, *Phys. Rev. E*, 2009, **79**, 021501.
41 S. H. Lee and C. M. Liddell, *Small*, 2009, **5**, 1957.
42 C. G. Shull, W. A. Strauser and E. O. Wollan, *Phys. Rev.*, 1951, **83**, 333.
43 F. Perrin, *J. Phys. Radium*, 1934, **5**, 497.
44 P. J. Flanders and J. P. Remeika, *Philos. Mag.*, 1965, **11**, 1271.
45 M. Reufer, H. Dietsch, U. Gasser, B. Grobety, A. M. Hirt, V. K. Malik and P. Schurtenberger, *J. Phys.: Condens. Matter*, 2011, **23**, 065102.
46 D. Hoffelner, M. Kundt, A. M. Schmidt, E. Kentzinger, P. Bender and S. Disch, *Faraday Discuss.*, 2015, **181**, 449.
47 F. Kun, W. Wen, K. F. Pal and K. N. Tu, *Phys. Rev. E*, 2001, **64**, 061503.
48 H. Morimoto, T. Maekawa and Y. Matsumoto, *Phys. Rev. E*, 2003, **68**, 061505.
49 T. Prokopyeva, V. Danilov, A. Dobroserdova, S. Kantorovich and C. Holm, *J. Magn. Magn. Mat.*, 2011, **323**, 1298.
50 T. A. Prokopieva, V. A. Danilov, S. S. Kantorovich and C. Holm, *Phys. Rev. E*, 2009, **80**, 31404.
51 E. C. Stoner and E. Wohlfarth, *J. Magn. Magn. Mat.*, 1948, **240**, 599.
52 A. V. Petrikevitch and Y. L. Raikher, *J. Magn. Magn. Mat.*, 1983, **39**, 79.
53 Y. L. Raikher and P. C. Scholten, *J. Magn. Magn. Mat.*, 1988, **74**, 275.
54 M. Belovs and A.Cbers, *Phys. Rev. E*, 2006, **73**, 051503.
55 K. Erglis, M. Belovs and A.Cebers, *J. Magn. Magn. Mater.*, 2009, **321**, 650.
56 A. Snezhko, I. S. Aranson and W. K. Kwok, *Phys. Rev. E*, 2006, **73**, 041306.
57 *Application of Magnetic Particles in Medicine and Biology*, ed. W. Andra, U. Hafeli, R. Hergt and R. Misri, John Wiley and Sons, Amsterdam, 2007.
58 A. Terray, J. Oakey and D. W. M. Marr, *Science*, 2002, **296**, 1841.
59 S. Bleil, D. W. M. Marr and C. Bechinger, *Appl. Phys. Lett.*, 2006, **88**, 263515.
60 N. Pamme, *Lab Chip*, 2006, **6**, 24.
61 T. Sawetzki, S. Rahmouni, C. Bechinger and D. Marr, *Proc. Natl. Acad. Sci. U.S.A.*, 2008, **105**, 20141.
62 B. Kavcic, D. Babic, N. O. B. Podobnik and I. Poberaj, *Appl. Phys. Lett.*, 2009, **95**, 23504.
63 S. L. Biswal and A. P. Gast, *Anal Chem.*, 2004, **76**, 6448.
64 T. G. Kang, M. A. Hulsen, P. D. Anderson, J. M. J. den Toonder and H. E. H. Meijer, *Phys. Rev. E*, 2007, **76**, 066303.
65 H. H. Himstedt, Q. Yang, L. P. Dasi, X. H. Qian, S. R. Wickramasinghe and M. Ulbricht, *Langmuir*, 2011, **27**, 5574.
66 Y. Gao, A. van Reenen, M. A. Hulsen, A. M. de Jong, M. W. J. Prins and J. M. J. den Toonder, *Microfluid Nanofluid*, 2014, **16**, 265.
67 Y. Gao, J. Beerens, A. van Reenen, M. A. Hulsen, A. M. de Jong, M. W. Prins and J. M. J. den Toonder, *Lab Chip*, 2015, **15**, 351.
68 A. Brasovs, J. Cimurs, K. Erglis, A. Zeltins, J. F. Berret and A. Cebers, *Soft Matter*, 2015, **11**, 2563.

This journal is © The Royal Society of Chemistry [year]